

THE RISE OF TWISTED MAGNETIC TUBES IN A STRATIFIED MEDIUM

F. MORENO-INSERTIS AND T. EMONET

Instituto de Astrofísica de Canarias, 38200 La Laguna (Tenerife), Spain; fmi@ll.iac.es, temonet@ll.iac.es

Received 1996 July 30; accepted 1996 September 10

ABSTRACT

First results from a two-dimensional numerical study of the buoyant rise of twisted magnetic flux tubes in the solar convection zone are presented. We show in detail the process by which the transverse component of the field can suppress the splitting of the rising tube into two vortex filaments. For the suppression to be effective, the pitch angle of the twisted field lines has to be above a threshold given by the condition that the magnetic equivalent of the Weber number (see § 2.2) be below 1. The shape obtained for the tube and wake is strongly reminiscent of laboratory experiments with air bubbles rising in liquids. The magnetized region outside an equipartition boundary is *peeled* away from the tube: two sidelobes are formed, which lag behind the tube and contain only a fraction of the initial magnetic flux. This is similar to the formation of a *skirt* in the fluid dynamical case. The velocities of rise predicted by the thin flux tube approximation are compared with those obtained here.

Subject headings: hydrodynamics — plasmas — magnetic fields — Sun: activity — Sun: interior

1. INTRODUCTION

There is increasing evidence, from both theory and observation, for the fact that the tubes which rise through the convection zone of the Sun are twisted before they appear at the surface. Observationally, there is evidence of a nonpotential configuration of the field in emerging magnetic regions (Lites et al. 1995; Leka et al. 1996), suggestive of a twist of the rising flux ropes before they appear at the surface (see also Tanaka 1991; Kurokawa 1989; Rust & Kumar 1996). There are several theoretical arguments in support of a nonzero twist of the magnetic tube progenitors of active regions. A non-twisted, buoyant tube is acted upon by gravitational torques along the rise and turns into a pair of vortex filaments rotating in opposite directions (Schüssler 1979; Longcope et al. 1996). The latter authors show in detail how the buoyancy force acting on the mass elements of the vortex filaments causes them to separate horizontally from each other. The rise is then stopped asymptotically and no flux emergence takes place. However, if the tube were twisted by a sufficient amount, the magnetic tension could prevent the formation of the vortex filaments. There are also indications of mechanisms producing twisted tubes. The two-dimensional case has been discussed by Cattaneo, Chiueh, & Hughes (1990). A Rayleigh-Taylor unstable slab of plasma with a horizontal magnetic field produces untwisted rising tubes, which develop sidelobes reminiscent of the vortex filaments in Longcope et al. (Cattaneo & Hughes 1988). However, when the magnetic layer has a nonuniform transverse component, the resulting tubes are twisted. In the more spectacular three-dimensional case (Matthews, Hughes, & Proctor 1995), an unstable layer with a parallel horizontal field produces magnetic tubes with nonzero vorticity. Through nonlinear interaction, these tubes arch as they rise in a vertical plane, thereby becoming twisted. Further arguments can be obtained through the general increase of the twist of a tube when it expands along the rise (Parker 1979, chap. 9).

In this Letter we report on the results of a calculation of the rise of twisted horizontal magnetic tubes in a stratified and compressible medium. We study a model problem which can be applied to magnetic tubes rising in the convection zone. A moderate amount of twist is shown to suppress the formation

of vortex filaments in the tube. The shape of the rising tube and its wake are strongly reminiscent of air bubbles rising in a liquid, with a clear dependence of the shape of both the bubble and the wake on the amount of twist. We also compare the speed of rise with predictions based on the thin flux tube approximation.

2. THE PHYSICAL PROBLEM

2.1. Equations and Initial Conditions

The system under consideration is a compressible and stratified plasma that obeys the general equations of magnetohydrodynamics (MHD) (mass conservation, momentum, and energy as well as the induction equation), including classical ohmic diffusion. Of particular importance for this Letter is the equation for the vorticity, $\boldsymbol{\omega} = \nabla \times \mathbf{v}$,

$$\rho \frac{D}{Dt} \left(\frac{\boldsymbol{\omega}}{\rho} \right) = (\boldsymbol{\omega} \cdot \nabla) \mathbf{v} - \nabla \left(\frac{1}{\rho} \right) \times \nabla p_{\text{tot}} + \nabla \times \mathbf{F}_L^c, \quad (1)$$

with p_{tot} the total pressure ($p + p_m$) and $\mathbf{F}_L^c = \{[\mathbf{B}/(4\pi\rho)] \cdot \nabla\} \mathbf{B}$. We use a Cartesian coordinate system (x, y, z) in which $\mathbf{g} = (0, 0, -g)$. Our system is two-dimensional in the sense that $\partial/\partial y \equiv 0$ (however, both B_y and v_y are generally nonzero). The resulting equations are solved using a code written by Shibata (1983), which is based on an explicit, modified Lax-Wendroff scheme (Rubin & Burstein 1967) including artificial viscosity. This code has been thoroughly tested and used for a number of astrophysical problems (see, e.g., Shibata 1983; Kaisig et al. 1990). We have modified the code in some respects to use it for the present problem and have run additional tests (see Emonet & Moreno-Insertis 1997).

The background atmosphere in our integration box (spanning 300×350 mesh points) is adiabatically stratified, with pressure and density denoted p_h and ρ_h , and has a pressure contrast between the top and bottom of the box of 2.6. At time $t = 0$ we superpose an axisymmetric magnetic flux distribution of the form

$$B^y \propto e^{-r^2/R^2}, \quad B^\phi \propto B^y (r/R)^3 e^{-r^2/R^2} \quad (2)$$

around a point in the lower part of the box (we call r and ϕ the polar coordinates around that point). In this way, the pitch angle decreases exponentially at large distances and has a maximum at a radius $r = (3/2)^{1/2}R$ (B_y there is about half its maximum value). We set the total pressure at time $t = 0$ equal to p_h . Finally, the entropy is assumed constant in the whole box. The magnetic region will then be buoyant, and, to first order in $1/\beta$,

$$\Delta\rho/\rho \stackrel{\text{def}}{=} (\rho - \rho_h)/\rho = -(\gamma\beta)^{-1}. \quad (3)$$

This case is intermediate between the two extreme possibilities of full thermal equilibrium (a factor of γ more buoyant) and the case of a tube with $\rho = \rho_h$. The evolution presented here is qualitatively very similar to the first case, whereas it deviates in important respects from the second (Emonet & Moreno-Insertis 1997). As boundary conditions we choose closed lids (sides and bottom of the box) and an open boundary with a fiducial layer at the top.

2.2. Physical and Numerical Parameters

The three main dimensionless parameters controlling the behavior of the rising magnetic tubes are (a) the plasma beta, (b) the *thickness* of the tube (as measured by, e.g., R/H_p), and (c) the degree of twist (e.g., the maximum pitch angle). The values we choose for those parameters represent a compromise between numerical feasibility and closeness to the solar case. The time step is limited by a Courant condition, so that $1/\beta$ and the tube radius cannot be too small. In fact, within a factor of $O(1)$ we have $N_t = N_z(\beta H_p/R)^{1/2}$, with N_z the number of cells in the vertical direction and N_t the number of necessary time steps. This provides a strict upper bound for β and H_p/R . In this Letter we use $\beta = 10^3$ and $R = 3.7 \times 10^{-2} H_p$, which are not too bad for the bottom of the convection zone, where field strengths up to $O(10^5 \text{ G})$ are expected (Moreno-Insertis 1992).

Values of interest for the third parameter, the pitch angle, can be estimated in two ways. The large β entails a slow subsonic rise and permits writing the second term on the right-hand side of equation (1) to leading order in the form

$$\nabla \left(\frac{\Delta\rho}{\rho_h} \right) \times \mathbf{g}, \quad (4)$$

which is also the term obtained in the Boussinesq limit (Longcope et al. 1996). Using equation (3), we gather that the magnetic stresses of the transverse field become dynamically important when the pitch angle, Ψ , reaches a value of order

$$\tan \Psi \gtrsim \left(\frac{R}{H_p} \right)^{1/2} \quad (5)$$

on average in the tube (see Tsinganos 1980; Emonet & Moreno-Insertis 1996). For the parameters used in the following section, this rough estimate yields an angle of about 10° . An alternative method of deriving this condition is to require that the magnetic tension force associated with the transverse field be able to withstand the pressure perturbations along the tube forefront associated with the buoyant rise. Defining the magnetic equivalent of the Weber number in our problem, W_m , as the ratio between the ram pressure of the external flow and the equivalent surface tension associated with the jump in magnetic stresses at the tube boundary, it can be seen that condition (5) is identical to requiring $W_m \lesssim 1$.

A further parameter is the magnetic Reynolds number, R_m , calculated on the basis of tube radius and rise speed. Steep magnetic gradients develop in the tube, especially at its front, so that relatively small values of R_m , like $R_m \sim 200$, are necessary for good numerical performance. However, they do not cause any substantial decrease of the quantity B_y/ρ at the tube center (which is constant in ideal MHD). In the following, the results are given in dimensionless form, using as units the background density, pressure scale height, and Alfvén speed calculated at the center of the tube at time $t = 0$.

3. THE SHAPE OF TUBE AND WAKE

If the pitch angle is much smaller than given in equation (5), then we obtain results similar to those of Schüssler (1979) and Longcope et al. (1996) for the untwisted case: the tube splits into two halves which make out a vortex filament pair, and the rise turns into a horizontal expanding motion. The behavior of the tube is completely different when the maximum of the pitch-angle distribution satisfies equation (5) (Fig. 1 [Pl. L8]). Since the tube center has the maximum buoyancy, the initial stages are characterized by the formation of a ribbon of field close to and parallel to the upper edge of the tube. A thin sheet of weak field above and on the sides of the ribbon is *peeled* off the tube toward the wake that forms at the rear. In this way two sidelobes are formed. Only a small amount of matter and flux is drained away from the tube; it comes from the region where the local magnetic energy of the transverse field is below the kinetic energy of the flow around the tube. This process is, in some sense, self-defeating in that it stretches and thus strengthens the transverse field of the layer being dragged, making it increasingly difficult for further material to be carried to the sidelobes. In the final configuration, the magnetic tube, in the form of a *cylindrical cap* followed by a well-developed wake, has reached a roughly constant terminal velocity of rise.

The effect of twist can be best understood by comparing cases with different values of the maximum pitch angle, Ψ_{\max} , at time $t = 0$. In Figure 2 (Plate L9) (*upper row*), we are showing the tube configuration at time $t = 5.8$ (an intermediate stage of the evolution presented in Fig. 1) for values of Ψ_{\max} of 20° (*left*), 10° (*center*), and 4° (*right*). The height reached by the tube is very similar in all three cases; the velocity of rise is determined primarily by the y -component of the field and by the initial tube radius, which are the same in all of them. On the other hand, the thickness of the *skin* peeled off the upper tube boundary by the external flow increases for smaller Ψ_{\max} . This confirms the prediction of equation (5). More precisely, the amount of magnetic flux contained in the *head* of the tube noticeably decreases along this series as compared to the total flux in the sidelobes (Fig. 3). Choosing a value of Ψ_{\max} below the range shown in Figure 3 (but still close to it), e.g., 1° , yields a total splitting of the rising tube into several pieces. However, the evolution described by Longcope et al. (1996) is only reproduced when Ψ_{\max} is well below that range.

The resulting shape is strongly reminiscent of the laboratory experiments on the rise of buoyant gas bubbles in liquids (Ryskin & Leal 1984; Hnat & Buckmaster 1976). The role of surface tension in the present case is played by the jump in the magnetic stress at the tube boundary; major differences, though, are the stronger stratification and the low value of the density deficit, $O(1/\beta)$, in our case. The comparison is best

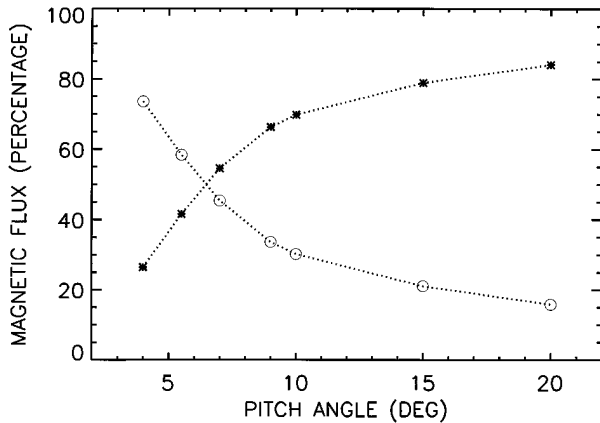


FIG. 3.—Asterisks: percentage of the initial magnetic flux that remains in the head of the tube at the end of the calculation as a function of Ψ_{\max} at time $t = 0$. Circles: the flux contained in the sidelobes.

understood by plotting the velocity field relative to the motion of the tube apex, v_{rel} , in the three cases shown in Figure 2 (see Fig. 2, lower row). The black dots encircling the tube have been drawn at the positions where the kinetic energy $\rho v_{\text{rel}}^2/2$ equals the magnetic energy of the transverse field (we will call the resulting curve the equipartition line). This plot reveals that the wake structure and the cylindrical cap shape are well-defined features: the motions in the tube interior (i.e., in the volume within the equipartition line) are much smaller than the relative motion of the tube as a whole with respect to the external medium. There is a noticeable dependence of the shape of the equipartition line on Ψ_{\max} : when the stiffness of the tube decreases, the shape of the frontal part remains roughly the same whereas the boundary to the wake changes from convex to concave. This asymmetry is basically due to two phenomena: (1) the differential buoyancy (Emonet & Moreno-Insertis 1996) in the tube increases (decreases) the transverse field above (below) the central magnetic O-point, and (2) additional resistance of the boundary layers on the upper edge of the tube is obtained through the stretching of the transverse field by the surrounding flow, as mentioned above. Thus, when Ψ_{\max} is small, the upper edge of the tube is still smooth and convex, whereas the wake can dent the lower boundary of the tube to a large extent.

The wake behind the tube is composed of two well-developed vortices: the no-slip condition at the tube surface is provided in our case by the magnetic field close to the equipartition contour. Outside this line (but close to it) there is vorticity generated and being advected by the external flow to the rear of the tube, where it accumulates and produces the vortices. The final shape of the volume occupied by the tube and wake is roughly that of an elliptical cylinder, with the tube taking up a larger fraction of the ellipse for higher values of Ψ_{\max} . The boundary of the wake is well delineated, with a clear separation line between rotational flow inside and largely nonrotational flow outside. The limiting streamline is approximately aligned with the transverse magnetic field, which has been stretched toward the wake of the tube. The latter feature is very similar to the thin trailing envelopes, or *skirts*, formed behind gas bubbles (Hnat & Buckmaster 1976).

4. VELOCITY

The rise speed of the tube as a whole is determined by the buoyancy force counteracted by the resistance of the sur-

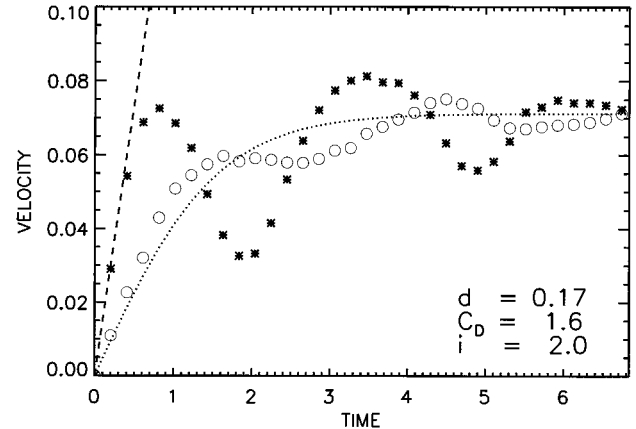


FIG. 4.—Velocities of the tube center v_c (asterisks), and of the apex of the tube v_t (circles). The dotted line, which corresponds to eq. (7), and the dashed line are explained in the text.

rounding medium. The reaction force of the surroundings to the translation motion of a cylinder of arbitrary cross section can be described using the aerodynamic drag formula $F_D = C_D \rho_h v^2 d/2$, with v the speed of the tube perpendicular to its axis and d the size of the cross section. C_D is the customary dimensionless shape coefficient. For a buoyancy-driven motion with constant density deficit and tube size, the resulting velocity follows a precise analytical law (e.g., Moreno-Insertis 1983):

$$v = v_{\text{ter}} \tanh(at/v_{\text{ter}}), \quad (6)$$

with the terminal velocity v_{ter} and the acceleration at time 0, a , given by

$$v_{\text{ter}} = \sqrt{\frac{g \int \Delta\rho dS}{C_D \rho_h d/2}}, \quad a = \left(\frac{g \int \Delta\rho dS}{i \int \rho dS} \right). \quad (7)$$

The factor i stems from the added inertia due to the external medium (it is equal to 2 for a rigid straight cylinder). In the case of our magnetic tube there are other phenomena taking place that are not included in equations (6) and (7). For instance, the center of the tube is more buoyant than the outer layers, therefore at the beginning it rises faster than the latter. The consequent increase in transverse field in the upper part of the tube decelerates this motion of the tube core so that, relative to the apex of the tube, the core reverses its motion. An oscillation of the tube core ensues with a frequency given, to order of magnitude, by the quotient of tube radius and Alfvén velocity of the transverse field.

In Figure 4 we show (asterisks) the instantaneous velocity of the tube center, v_c (defined as the O-point of the transverse field lines), and (circles) the velocity of the apex of the tube, v_t . These plots correspond to the run with $\Psi_{\max} = 10$. The velocity v_c is seen to oscillate around v_t , as expected. In fact, the velocity of the apex, which reflects the motion of the tube as a whole, also oscillates in response to the core motions. Both oscillations are damped, mainly because they are being radiated away to the outside medium, and approach an asymptotic terminal velocity given by equation (7) with $C_D = 1.6$ (right end of the dotted line). The initial slope of the velocity curves

can also be understood: for v_r , it is quite close to a (eq. 7) calculated with $i = 2$ and the densities at time $t = 0$; for v_c the initial acceleration is $(|\Delta\rho/\rho|)_{r=0} g/i$, again with $i = 2$ (*dashed line*). The rest of the dotted line is an interpolation designed to fit initial acceleration and terminal velocity: it is equation (6) with a calculated at time $t = 0$ and v_{ter} calculated for the asymptotic state. This curve makes apparent the global oscillations of the tube.

5. DISCUSSION AND CONCLUSIONS

The results shown in this paper indicate that twisted tubes may inhibit their conversion into a vortex filament pair when the transverse field is close to the value given in equation (5). An immediate question concerns the *persistence* of this effect or, in other words, what will happen to a rising tube in the convection zone once it has gone beyond the first few pressure scale heights. A partial answer is possible within the framework of this paper: the magnetic tubes presented here stop shedding magnetic flux to the wake at about the same time that the latter has come to full development. From then on the magnetic flux within the *equipartition boundaries* remains basically constant. In other words, the magnetic tube maintains its coherence, at least as long as no new phenomena come into play. One of these is the increasing effect of the outside stratification: in the convection zone, the decreasing temperature causes the scale heights to become very small in higher levels. The rapidly decreasing pressure and density in the rising tube bring about a general weakening of the field (B' goes down proportionally to ρ , at least for not too low magnetic Reynolds numbers). At the same time, the tube expansion produces an increase in the degree of twist in the

tube. The combination of these two processes (with possible kink instabilities, etc., in the three-dimensional case) may decide the fate of the tube in the uppermost layers of the convection zone.

The calculations presented here consider a magnetic flux tube that is substantially buoyant from the outset (it had the same entropy as the background). This has been done not only for reasons of numerical expediency but also because the gravitational torque is more effective the larger the initial density deficit (eq. 4). Thus, it is the best case to understand the inhibition of the formation of vortex filaments by the transverse field. For many cases, one actually expects the rising tubes to be less buoyant than as given by equation (3), e.g., if they are Parker-unstable tubes starting from an equilibrium condition (Caligari, Moreno-Insertis, & Schüssler 1995). A simple calculation shows that, for a fixed vertical distance traversed by the tube, one needs a much smaller amount of twist to suppress the formation of vortices in the tube in this case than in the isothermal or isentropic problems. On the other hand, the internal dynamics of the rising two-dimensional tube is also substantially different in this case. A detailed numerical study is thus necessary to obtain definite results.

This work was partially funded through the DGICYT project C91-0530. Permission to use the parallel-computing facilities of CEPBA (Barcelona, Spain) and the Cray computers at CIEMAT (Madrid, Spain) is gratefully acknowledged. We are also grateful to M. Schüssler, M. Kaisig, and K. Shibata for interesting comments and discussions.

REFERENCES

- Caligari, P., Moreno-Insertis, F., & Schüssler, M. 1995, ApJ, 441, 886
 Cattaneo, F., Chiueh, T., & Hughes, D. W. 1990, J. Fluid Mech., 219, 1
 Cattaneo, F., & Hughes, D. W. 1988, J. Fluid Mech., 196, 323
 Emonet, T., & Moreno-Insertis, F. 1996, ApJ, 458, 783
 ———. 1997, in preparation
 Hnat, J. G., & Buckmaster, J. D. 1976, Phys. Fluids B, 19, 2, 182
 Kaisig, M., Tajima, T., Shibata, K., Nozawa, S., & Matsumoto, R. 1990, ApJ, 358, 698
 Kurokawa, H. 1989, Space Sci. Rev. 51, 49
 Leka, K. D., Canfield, R. C., McClymont, A. N., & van Driel-Gesztelyi, L. 1996, ApJ, 462, 547
 Lites, B. W., Low, B. C., Martínez Pillet, V., Seagraves, P., & Skumanich, A. 1995, ApJ, 446, 877
 Longcope, D. W., Fisher, G. H., & Arendt, S. 1996, ApJ, 464, 999
 Matthews, P. C., Hughes, D. W., & Proctor, M. R. E. 1995, ApJ, 448, 938
 Moreno-Insertis, F. 1983, A&A, 122, 241
 ———. 1992, in Sunspots, Theory and Observations, ed. J. H. Thomas & N. O. Weiss (Dordrecht: Kluwer), 385
 Parker, E. N. 1979, Cosmical Magnetic Fields (Oxford: Oxford Univ. Press)
 Rubin, E. L., & Burstein, S. Z. 1967, J. Comput. Phys., 2, 178
 Rust, D. M., & Kumar, A. 1996, ApJ, 464, L199
 Ryskin, G., & Leal, L. G., 1984, J. Fluid Mech., 148, 19
 Schüssler, M. 1979, A&A, 71, 79
 Shibata, K. 1983, PASJ, 35, 263
 Tanaka, K. 1991, Sol. Phys., 136, 37
 Tsinganos, K. C. 1980, ApJ, 239, 746

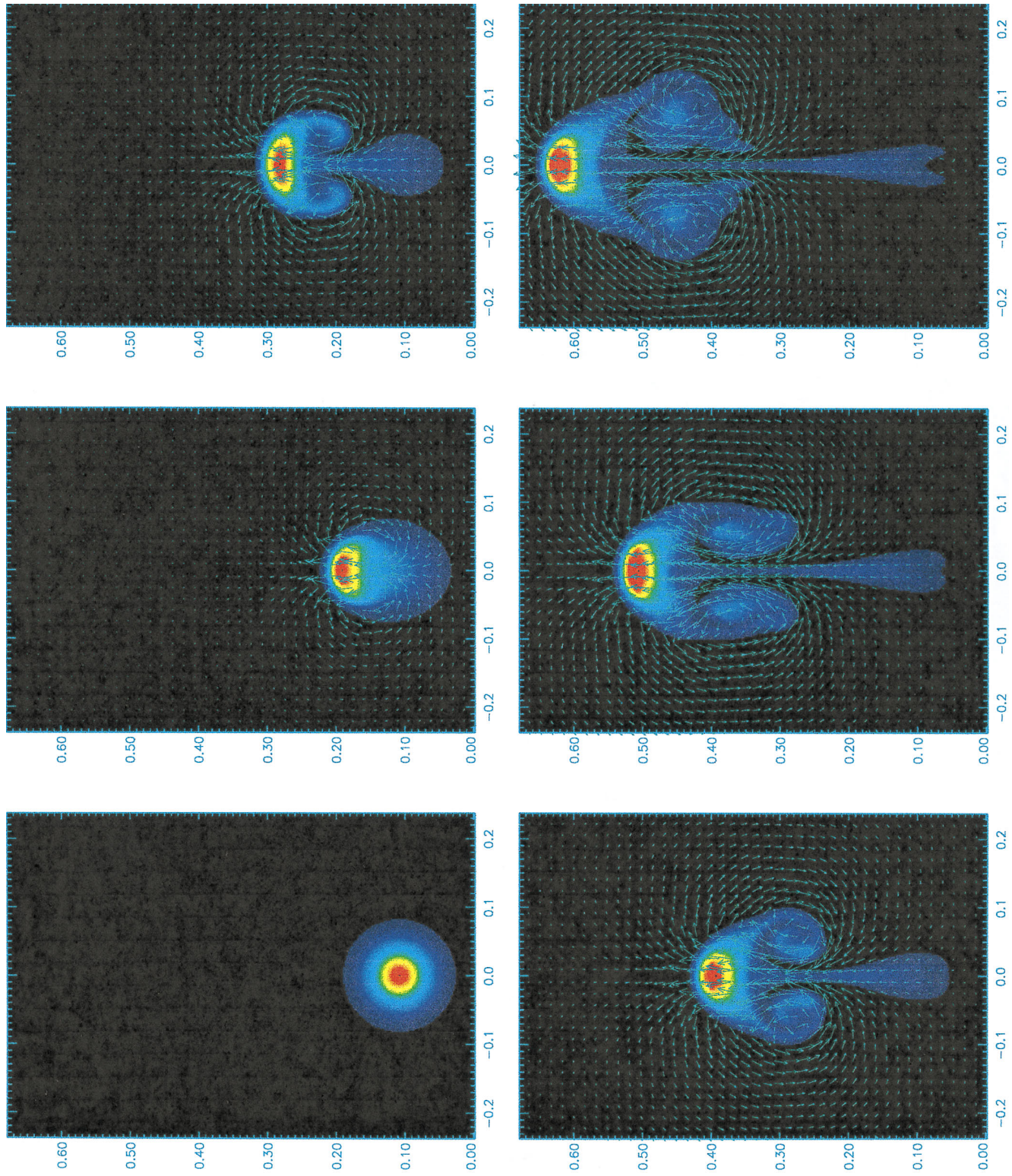


FIG. 1.—Rise of a twisted magnetic flux tube with $\Psi_{\max} = 10$ at $t = 0$. The six views are regularly spaced in time between $t = 0$ and $t = 8.2$. The color scale refers to the intensity of the longitudinal magnetic field; the maximum in each panel is red; deep blue is 10% of the maximum, black is less than 1%. The arrows indicate the instantaneous velocities. Their length is normalized to the maximum velocity at time $t = 8.2$. The panels show only a fraction (200×300 points) of the integration box used in the calculation, which contained 300×350 equally spaced nodes.

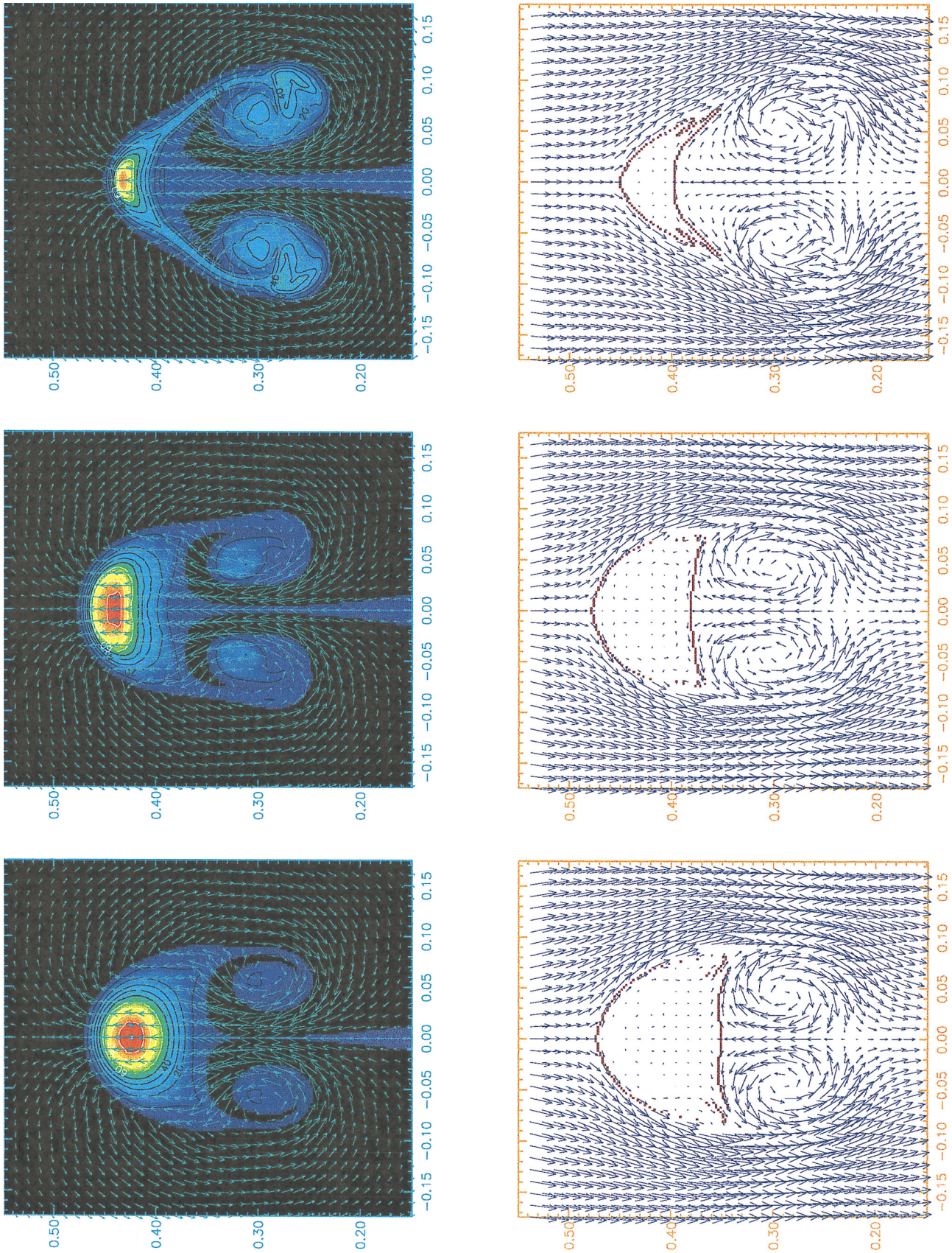


FIG. 2.—Upper row: B^y distribution at time $t = 5.8$ for values of Ψ_{\max} of 20° (left), 10° (center), and 4° (right). The color index and velocities are scaled to the case $\Psi_{\max} = 20$ (right). Only the central section of the integration box (150×170 nodes) is shown. Lower row: the velocity field relative to the motion of the tube apex, v_{rel} , is plotted for the same three cases of the upper row. The dark brown dots encircling the tube have been drawn at the positions where $\rho_{\text{rel}}^2/2 = B_l^2/8\pi$.